ACS APPLIED NANO MATERIALS

www.acsanm.org Article

Substrate-Dependent Growth Mode Control of MoS_2 Monolayers: Implications for Hydrogen Evolution and Field-Effect Transistors

Min-Yeong Choi,[§] Chang-Won Choi,[§] Seong-Jun Yang, Hojeong Lee, Shinyoung Choi, Jun-Ho Park, Jong Heo, Si-Young Choi,* and Cheol-Joo Kim*

Cite This: *ACS Appl. Nano Mater.* 2022, 5, 4336−4342 Read Online

ACCESS | Metrics & More | Article Recommendations | Supporting Information

ABSTRACT: The control of domain sizes provides a powerful means to engineer the characteristics of monolayer (ML) MoS_2 films for specific applications including catalysts for hydrogen evolution and thin-film transistors. Here, we report an efficient way to control domain structures of MoS_2 by substrate-dependent growth mode control. Deterministic control of growth modes, associated with catalytic intermediates, is introduced by utilizing different growth substrates in metal−organic chemical vapor deposition (MOCVD) of ML MoS_2. Na-Mo-O eutectic alloys formed by a soda lime (SL) substrate dominate the growth based on a vapor−liquid−solid (VLS) process, resulting in large-crystalline domains of MoS_2 with a reduced density of liquid nuclei. On the other hand, MoO_{3-x} seeds formed from an alkali aluminosilicate (AA) substrate accelerate nucleation via a vapor−solid−solid (VSS) process for nanocrystalline domains. ML MoS_2 of nanocrystalline domains resulted in efficient hydrogen evolution reactions (HERs), while large-domain films showed better electron conductivity.

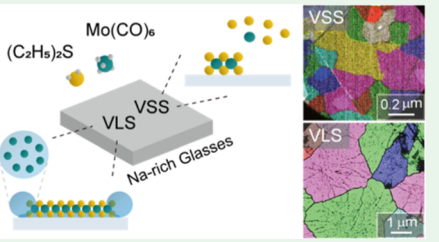

KEYWORDS: *metal−organic chemical vapor deposition, MoS_2, catalyst, vapor−liquid−solid growth, vapor−solid−solid growth, domain structures, glass substrates*

INTRODUCTION

Metal−organic chemical vapor deposition (MOCVD) provides an effective way to directly grow two-dimensional (2D) transition metal dichalcogenide (TMDC) films with large-scale uniformity on arbitrary substrates.[1] The films can be used as thin-film transistors with high carrier mobility,[2] active optoelectric components with high quantum yield,[3,4] nonlinear media with high optical susceptibilities,[5,6] and catalytic agents for hydrogen evolution reactions (HERs).[7] Depending on the specific application, a TMDC film has been modified to exhibit a particular microstructure by the control of various parameters such as temperature, pressure, flow rate of gaseous precursors, and so on. To this end, catalysts play key roles in controlling the growth kinetics and the resultant microstructures of TMDCs. For example, alkali metals as a catalytic element have been widely used to promote the fast growth rate and suppress nucleation, giving rise to the large domain size. However, the underlying mechanism by which catalysts control the crystalline structures is still ambiguous due to complex variables that affect the growth and nucleation.[8−13]

One main reason for the complexity is the fact that different catalytic intermediates can be formed from the same alkali element.[14] In particular, growth modes can change between vapor−liquid−solid (VLS) and vapor−solid−solid (VSS) modes with completely different nucleations and growth kinetics, depending on the phase of intermediates through which vapor-phase precursors react to form solid films. For example, eutectic intermediates such as sodium molybdate (Na_2MoO_4, $Na_2Mo_2O_7$, $Na_2Mo_4O_{13}$) that contain alkali metal form liquid alloys, within which nucleation and catalyst-assisted growth occur by supersaturation of precursor elements.[12,13,15] On the other hand, solid-state intermediates such as molybdate (MoO_x) lead to the VSS mode. In this case, solid-surface diffusion of ad-molecules from vapor and attachment to solid seeds are the rate-determining steps for growth and nucleation, which can be accelerated by the existence of alkali metals nearby.[16−20] A systematic comparison of VLS and VSS growth modes with different intermediates provides useful information for the different functions of each catalytic agent and a catalyst-assisted growth method to effectively control the domain structures of 2D TMDCs. However, the deterministic control of the chemical reactions to fabricate targeted catalytic intermediates is difficult to achieve by simply modulating the growth conditions such as temperature and pressure in MOCVD.

RESULTS AND DISCUSSION

We utilized various growth substrates with different chemical compositions (Table S1 in the Supporting Information) to

Received: January 25, 2022
Accepted: February 25, 2022
Published: March 9, 2022

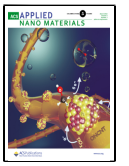

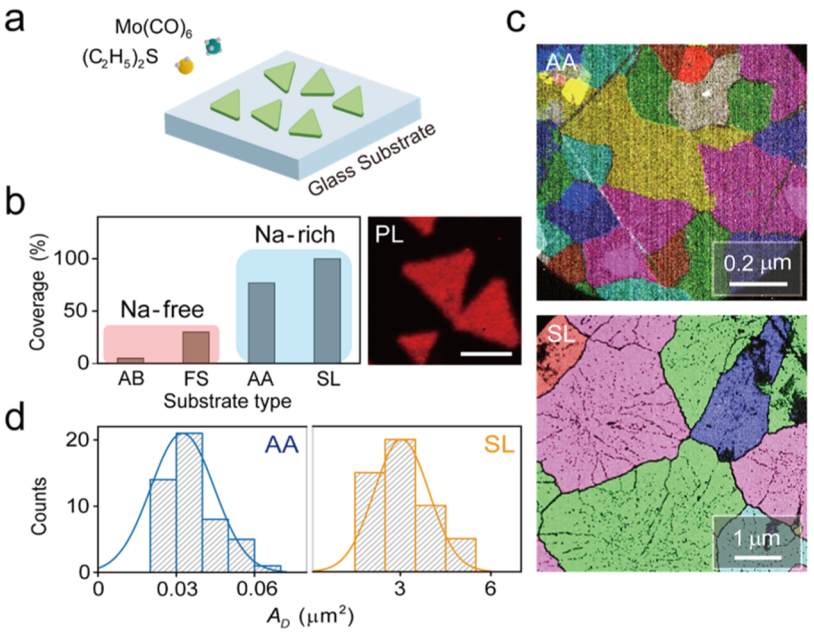

Figure 1. Growth substrate-dependent crystalline structures of ML MoS_2. (a) Schematics of MoS_2 growth by MOCVD. (b) Surface coverage of MoS_2 grown on different glass substrates (AB, alkali-free boro-aluminosilicate; FS, fused silica; AA, alkali aluminosilicate; and SL, soda lime) under the same growth conditions; right: PL image with excitation of 1.85 eV on a partially grown sample. Scale bar: 10 μm. (c) False-color DF-TEM images of polycrystalline MoS_2 films grown on AA and SL glass substrates. (d) Distributions of crystalline domain sizes of each MoS_2 film.

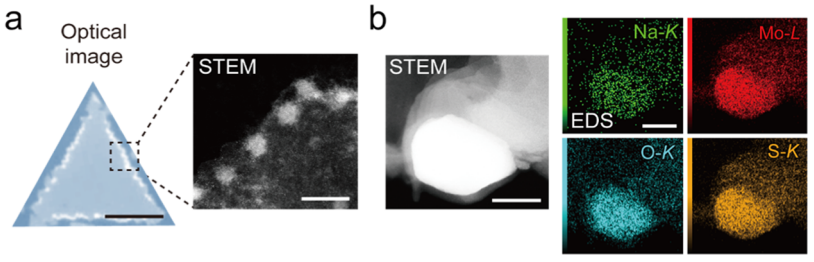

Figure 2. Catalyst-driven growth of MoS_2 crystals. (a) Optical image of discrete ML MoS_2 grown on a SL glass substrate. Scale bar: 20 μm. (Inset image) High-angle annular dark-field (HAADF)-STEM images of eutectic alloy magnified at each groove. Scale bar: 10 nm. (b) STEM and EDS mapping images for Na-K, Mo-L, O-K, and S-K from a eutectic alloy. Scale bar: 50 nm. (For the intense EDS signals of elements in (b), we carried out EDS elemental mapping for the larger particle than that of the inset image in (a)).

control the formation of catalytic intermediates in MOCVD of ML MoS_2 (Figure 1a) (see Figure S1 for confirmations of ML thickness in continuous films). In particular, two different glass substrates of soda lime (SL) glass and alkali aluminosilicate (AA) with similar Na contents (~10%) were used to grow ML MoS_2 at the same growth conditions. Growths on both SL glass and AA substrates showed significantly higher surface coverages of ML MoS_2 (Figure 1b, left) in optical absorption and photoluminescence (PL) imaging (Figure 1b, right) than the reference samples grown on Na-free glass substrates (Figure 1b, left), suggesting that Na is a key catalyst for the fast growth of MoS_2.[16] On the other hand, different domain sizes were observed between samples grown on SL glass and AA, despite the same growth conditions. Dark-field transmission electron microscopy (DF-TEM) images of polycrystalline films with full coverage (Figure 1c) show roughly 100 times larger grain sizes on SL glass than on AA (Figure 1d), demonstrating different growth kinetics between SL glass and AA substrates. This observation is surprising because previous reports show similarly enlarged MoS_2 domains with the existence of Na, regardless of the source precursors for Na.[11]

We examined the possible formations of different catalytic intermediates on each substrate by characterizing the microstructures of MoS_2. An optical image of partially grown MoS_2 on SL glass showed lines with bright contrasts along the edges of triangular domains (Figure 2a), which were absent in samples grown on AA. Scanning transmission electron microscopy (STEM) imaging at each edge of the discrete MoS_2 revealed that discrete particles exist along the edge (inset image mapping by STEM energy-dispersive X-ray spectroscopy (EDS) in Figure 2a, image on the left-hand side in Figure 2b). Elemental mapping by STEM-EDS showed that the particles are Na-containing alloys (K edge) with Mo (L edge), O (K edge), and S (K edge) (images on the right-hand side in Figure 2b). In contrast, STEM images of MoS_2 domains grown on AA did not show the alloy with excess elements compared to the surroundings (Figure S2). The existence of Na-Mo-O alloys on all of the edges of MoS_2 grown on SL glass suggests that the alloys functioned as the nucleation seeds and growth fronts.

The formations of different catalytic intermediates and their roles were further investigated by separating the intermediate formation and MoS_2 growth steps. Na-containing compounds were first formed by flowing only $Mo(CO)_6$ as a Mo precursor

https://doi.org/10.1021/acsanm.2c00369
ACS Appl. Nano Mater. 2022, 5, 4336−4342

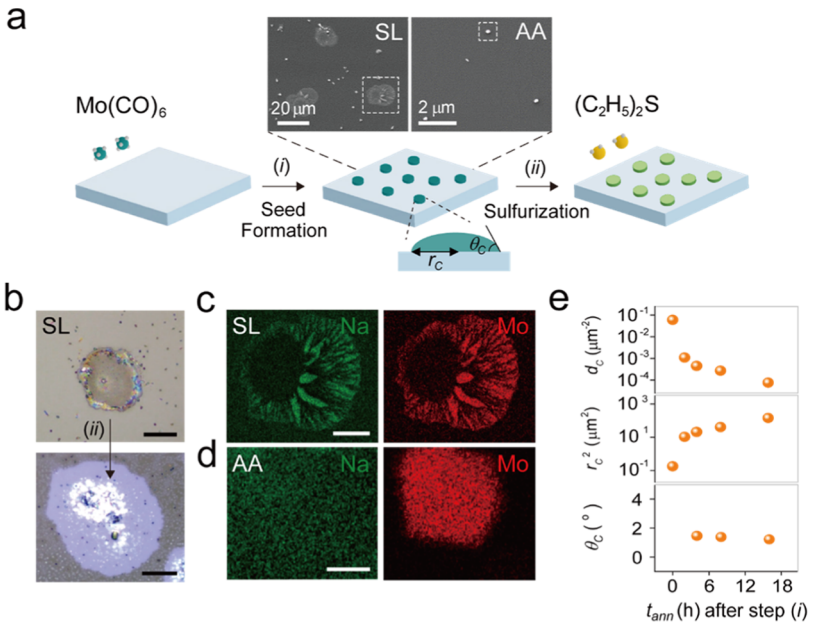

Figure 3. Substrate-dependent nucleation seeds. (a) Schematics for the two-step growth of MoS_2: (i) formation of Mo-containing nucleation seeds and (ii) conversion of the seeds to MoS_2 by sulfurization. Upper insets: SEM images on SL and AA substrates after step (i) and lower inset: schematic of a single seed, where θ_c is the contact angle between the seed and the surface and r_c is the radius of the seed. (b) Optical images of a seed on SL before and after step (ii). Scale bar: 20 μm. (c, d) EDS elemental mappings for Na and Mo by SEM near the seeds on (c) SL and (d) AA substrates, highlighted by the dashed box in a. Scale bar: (c) 5 μm and (d) 0.2 μm. (e) Change of d_c, r_c^2, and θ_c as a function of t_{ann} after step (i).

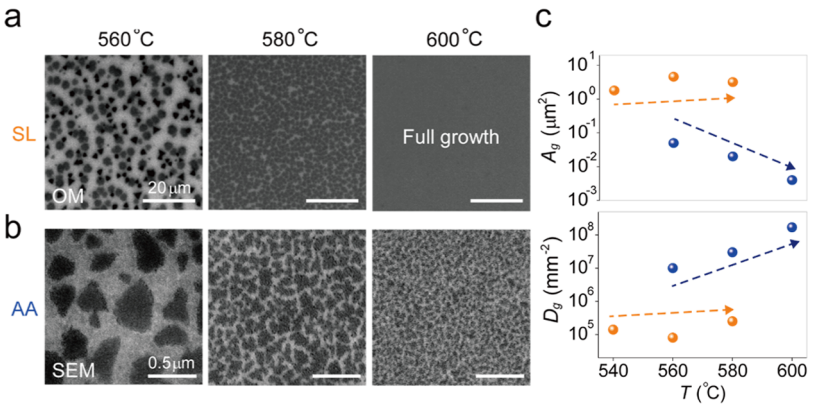

Figure 4. Growth temperature-dependent domain structure of ML MoS_2 on SL and AA surfaces. (a, b) Representative optical and SEM images of as-grown MoS_2 on (a) SL and (b) AA substrates with different growth temperatures. (c) Area A_g and density of grain D_g for MoS_2 on SL (orange) and AA (blue) versus growth temperatures.

to react with Na in the substrates under an Ar/H_2 atmosphere at 600 °C (Figure 3a). Annealing of the substrates after the introduction of $Mo(CO)_6$ resulted in particles on the surfaces of both SL glass and AA (Figure 3a, upper inset). Subsequent sulfurization by flowing only $(C_2H_5)_2S$ as a S precursor under the same atmosphere and temperature transformed the particles to MoS_2 crystals (Figure 3b), as confirmed by PL and Raman spectra (Figure S3), demonstrating that the particles provided nucleation seeds.

The chemical compositions of the seed particles were different on SL than on AA. Elemental mapping (Figure 3c,d) by EDS spectra (Figure S4) showed that the seeds are Na-Mo-O alloy on SL substrate and molybdenum oxide (or extremely Na-poor Na-Mo-O alloy) on AA substrate. In addition, we found that the density d_c of the catalytic seed particles was much lower on SL substrates ($\sim 10^{-4}$ seed/μm^2) than on AA substrates ($\sim$25 seed/μm^2) after annealing for 4 h; this difference implies that different d_c values are the origin of the different domain-size distributions in the full-coverage films (Figure 1c,d). On the SL substrate, increasing the annealing time (t_{ann}) further reduced d_c, enlarged the average radius r_c of the particles, and maintained a constant low contact angle θ_c of $\sim$1.35° (Figure S5) on the surface of SL (Figure 3c). On the AA substrates, an increase in t_{ann} did not induce such morphological evolution of particles; therefore, they usually formed faceted crystals, whereas crystals on SL were rounded.

At the growth temperature, the Na-Mo-O alloys that serve as nucleation seeds form a liquid with a decreased eutectic temperature of $\sim$500 °C,[11] whereas MoO_x remains solid. Therefore, Na-Mo-O alloys can have a low θ_c and diffuse effectively over the surface. As t_{ann} increases, r_c^2 initially increases rapidly, then saturates; this behavior is characteristic

https://doi.org/10.1021/acsanm.2c00369
ACS Appl. Nano Mater. 2022, 5, 4336−4342

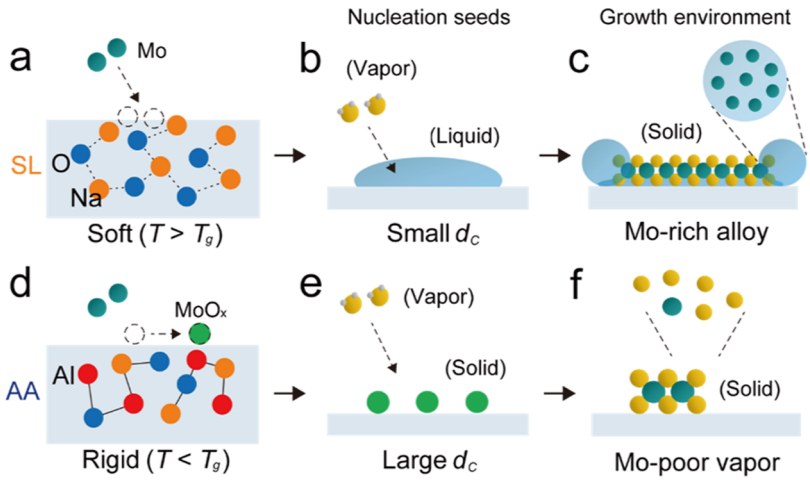

Figure 5. Schematics for catalyst-driven growths of MoS_2. (a–c) VLS growth mode on SL substrates. (a) Formation of Na-Mo-O eutectic liquid alloy by chemical reactions between thermally decomposed Mo precursors and Na and O from a soft medium at a temperature higher than T_g. (b) Nucleation by supersaturation of sulfur in the liquid alloy. The density of alloys is small due to Ostwald ripening. (c) Growths within the Mo-rich environment of Na-Mo-O alloy. (d-f) VSS growth mode on AA substrates. (d) Formation of solid-state MoO_x by aggregation of surface-diffusive, volatile MoO_x. Reactions between Mo and Na and O from the substrate are not activated at a temperature lower than T_g. Aluminum contents in the glass increase T_g. (e) Nucleation by reactions between vaporized sulfur and MoO_x. The nonaggregated MoO_x seeds have a high density. (f) Growths in a Mo-poor environment due to the low vapor pressure of Mo precursors.

of particle evolution by Ostwald ripening (Figure 3e).[21] This observation contradicts the previously proposed mechanism,[11] where high surface mobility of the eutectic intermediates reduced the number of nuclei by the merging of separated intermediates. Our results suggest that the reduction in the number of nuclei occurs by sequential dissolution and redeposition of the liquid particles, rather than by their direct coalescences. Therefore, d_c can decrease during the early stage of the growth prior to nucleation; therefore, the resulting domains are large, even when Mo and S precursors are injected simultaneously. During the growth at temperatures above the eutectic temperature of the intermediates, they become supersaturated with S, leading to MoS_2 growth by the VLS mechanism.[13] The growth proceeded with continuous liquid alloys, surrounding all of the edges; then, the alloys divide into segregated solid particles upon cooling, as shown in Figure 2b. If the continuous MoS_2 film completely passivates the surface to block the reaction between the Mo precursor and the Na-containing substrate, the remaining Na-Mo-O alloys are removed by evaporation at high growth temperature without further formation (see Figure S6 for an optical image of a continuous as-grown MoS_2 film on SL without alloys and schematics for the process). The difference in domain sizes of MoS_2 grown on SL and AA substrates can further increase by modulating the growth temperatures in the high-condensation regime with a large supply of precursors (Figure 4a,b). On SL substrates, temperature increases caused relatively small changes in the average sizes A_g and densities D_g of grains in the partially covered MoS_2. On AA substrates, temperature increases caused a decrease in A_g and an increase in D_g (Figure 4c). As a result, the same growth conditions on SL and AA, both of which have Na of ∼10%, can yield similar MoS_2-surface coverage but grain sizes that are 160 times larger on SL than on AA; therefore, domains on MoS_2 have large crystals (domain size ∼ 3.2 μm^2) on SL and nanocrystals (∼0.02 μm^2) on AA. The different temperature dependencies of A_g and D_g between SL and AA result from the different growth modes. On SL, nucleation occurs by supersaturation of liquid Na-Mo-O catalysts by the VLS mechanism. Therefore, D_g is set by d_c, and the relationship should show a weak temperature dependence by two conflicting effects of temperature to determine d_c: an increase in temperature promotes thermal decompositions of precursors and Na exsolutions from the substrate, thereby leading to an increase in the number of intermediates formed, but they can easily aggregate to have similar d_c by increased surface diffusion before the nucleation of MoS_2.[22] On the other hand, the growth on AA follows the "hit and stick" picture of the surface diffusion-limited aggregation model by the VSS mechanism.[23,24] Nucleation occurs when the critical nucleus size is smaller than the total number of Mo within the surface-diffusion area at an equilibrium condition (Figure S7). In the model, the number of adsorbates increases with the temperature by increased thermal decompositions of precursors; therefore, D_g increases.

Now, we discuss why SL and AA substrates with the same quantity of Na can result in different catalytic intermediates and growth modes. By thermal decomposition of Mo precursors, Mo can react with both oxygen and Na from the growth substrates to form intermediate compounds. SL and AA have a similar amount of Na, but AA has a higher glass transition temperature (630 °C) than SL (570 °C) by the chemical compositions with higher Al_2O_3 contents (Table S1). Therefore, incorporating Mo into the rigid AA structure at the growth temperature of 600 °C becomes difficult, producing solid MoO_x (Figure 5a,d), while Na-Mo-O alloys are formed on SL with effective reactions between Mo and Na. We note that in a previous study,[8] growth of MoS_2 with elemental Mo precursors on SL did not show the formation of alloys. This is probably because the concentration of elemental Mo is high enough to promote efficient nucleation of Mo clusters instead of forming Na-Mo-O alloys, while the amount of thermally decomposed Mo precursors on the surface is much lower in our case; therefore, they are incorporated into the underlying substrate before forming the stable nucleus. We found that while the different intermediates on each substrate change the morphology of MoS_2 domains, the growth rates are similarly enhanced on both SL and AA by the presence of Na contents from the growth substrates, regardless of the types of

https://doi.org/10.1021/acsanm.2c00369
ACS Appl. Nano Mater. 2022, 5, 4336–4342

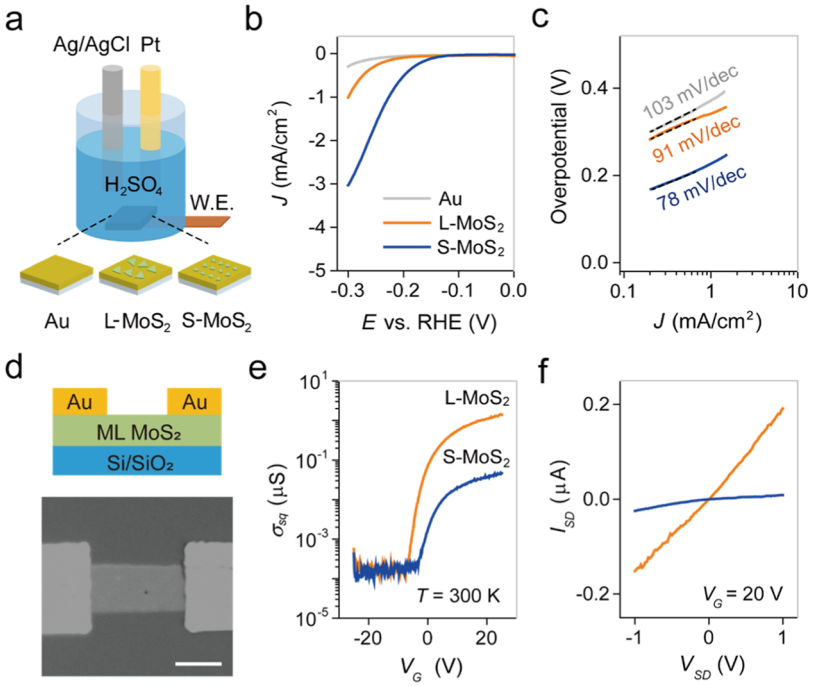

Figure 6. Domain structure-dependent catalytic activity and electrical properties of MoS_2. (a) Schematics of a three-electrode electrochemical cell for HER measurements. Three different working electrodes (bare Au, L-MoS_2-coated Au, and S-MoS_2-coated Au) were used for the measurements. (b) Linear sweep voltammetry curves for different working electrodes. (c) Tafel plots of the corresponding curves in b. (d) Schematic and optical image of a field-effect transistor with a ML MoS_2 channel. Scale bar: 10 μm. (e) Gate-dependent sheet conductance (σ_{sq}) for L-MoS_2 and S-MoS_2. They were measured by a source−drain bias of 0.5 V at vacuum conditions. (f) On-state $I-V$ curves of L-MoS_2 and S-MoS_2 channels at a gate bias of 20 V.

intermediates. In summary, the type of Na-containing glass substrates determines how Na elements affect the growth of MoS_2 rather than the total amounts of Na involved in the growth reactions.

The deterministic growth modes by formation of different intermediates have two important consequences on the growth of MoS_2. First, as discussed above, the domain sizes can be controlled over the broad range from nanocrystalline domains to several micrometer domains, which cannot be easily achieved with a simple modulation of growth parameters (temperature, pressure, and flow rate of gaseous precursors) of MOCVD. (Figure 5b,e). For instance, growth in the low-condensation regime with a small amount of precursor often results in large domain structures with limited D_g, but the growth rate becomes extremely slow (Figure S8a). In contrast, increasing the supply of precursors leads to fast growth, but the domain sizes become small (Figure S8b). Our results show that both large-domain (L-MoS_2) and small-domain MoS_2 (S-MoS_2) films can be obtained in the high-condensation regime by formations of appropriate growth intermediates. Second, growths in each case can occur in completely different chemical environments to provide additional variety in the microstructures of resultant MoS_2 (Figure 5c,f).[25,26] For instance, the Na-Mo-O droplets can serve as nanoscale chambers with high chemical potentials of Mo, which is difficult to achieve in the vapor phase due to the low vapor pressure of Mo precursors.

With the deterministic control of growth modes, we demonstrated structural programming of the characteristics of MoS_2 films for specific applications. MoS_2 films with L-MoS_2 and S-MoS_2, grown on SL and AA substrates, were compared for their catalytic activities and electrical properties. First, we performed HER in an electrochemical cell with Au working electrodes, on which partially grown MoS_2 (coverage ~ 80%) was placed (Figure 6a). The existence of MoS_2 significantly increased the HER catalysis with increased current densities and decreased overpotential thresholds; these results indicate that the MoS_2 functioned as an electrocatalyst (Figure 6b,c). S-MoS_2 had a higher catalytic effect than L-MoS_2, as supported by the drop of the onset voltage from 237 to 168 mV at a current density of 0.2 mA cm^{-2} and the Tafel slope from 91 to 78 mV dec^{-1}. These results are comparable with a previous report, in which domain structures of MoS_2 were engineered to increase the number of boundaries that have catalytic activity.[7] We attribute the pronounced HER with S-MoS_2 to its large number of active edges sites. In contrast, electrical transport, which can be suppressed by electron scattering at grain boundaries, was more efficient in L-MoS_2 than in S-MoS_2. In field-effect transistors that had a back gate (Figure 6d), MoS_2 films with an average single-domain size of 15 μm^2 exhibited on-state conductivities that were about 30 times higher than those in films that had an average domain size of 0.3 μm^2 (Figure 6e,f). The measurements were conducted in a two-probe configuration with the same device geometry.

CONCLUSIONS

In summary, we found that glass substrates with different chemical compositions can be utilized to determine the growth mode for MoS_2 films from vapor-phase precursors. While the existence of Na in the substrates similarly enhanced the total growth rate by catalytic activities, the reactions between Na and the growth precursors strongly depended on the reactivity of growth substrates, resulting in either liquid for VLS growth

https://doi.org/10.1021/acsanm.2c00369
ACS Appl. Nano Mater. 2022, 5, 4336−4342

or solid intermediates for VSS growth. By utilizing various Na-containing glasses to determine the growth modes, we can effectively modulate the crystalline structures of TMDCs even in the same growth conditions. Our results on the mode-dependent growth kinetics provide useful insights to control microstructures of 2D TMDCs in direct growths on different substrates for various potential applications.[27]

EXPERIMENTAL SECTION

Growth of ML MoS_2 by MOCVD. Growths were performed in a 4.5 inch (inner diameter) hot-wall quartz tube furnace. Glass substrates were rinsed with deionized water and blown dry using N_2, then placed in the chamber. Molybdenum hexacarbonyl ($Mo(CO)_6$, Sigma-Aldrich 577766) and diethyl sulfide ($(C_2H_5)_2S$, Sigma-Aldrich 107247) were introduced into the chamber as Mo and S sources, respectively, together with H_2 and Ar through separate lines. Samples in Figure 1b were grown by flowing $Mo(CO)_6$ (0.4 sccm), $(C_2H_5)_2S$ (3 sccm), H_2 (3 sccm), and Ar (500 sccm) with a total pressure of 10 Torr at 600 °C for 16 h. Samples in Figure 4 were grown by changing the growth temperatures with the same flow rates of precursors as those used for samples in Figure 1b. For samples in Figure 6, S-MoS_2 samples with partial coverage were grown on AA substrates by flowing $Mo(CO)_6$ (0.26 sccm), $(C_2H_5)_2S$ (1 sccm), H_2 (4 sccm), and Ar (500 sccm) with a total pressure of 10 Torr at 700 °C for 14 h. To obtain full-coverage samples, the growth time was increased to 18 h. L-MoS_2 samples were grown on SL substrates by the same growth conditions for 14 h, except for the growth temperature of 650 °C. For the full-coverage sample, the growth time was increased to 18 h. Samples in Figure 1c were grown by the same growth conditions as samples of Figure 6.

Transfer of MoS_2. To transfer MoS_2 to the target substrate, we spin-coated poly(methyl methacrylate) (PMMA, 495 K, 4 A) on as-grown samples at a speed of 4000 rpm for 1 min, then baked them at 180 °C for 10 min. The edge of the coated film was scratched with a knife, then the film was gradually dipped into deionized water with tilting. The PMMA/MoS_2 stack was delaminated from the surface by the water penetrating the interface and then floated to the water surface. The film was scooped with a target substrate, then annealed at 60 and 80 °C for 10 min and at 180 °C for 30 min to remove water and make conformal contact between MoS_2 and the target surface. Finally, PMMA was removed by dipping in acetone for a few hours.

TEM Characterizations. ML MoS_2 was suspended on a Quantifoil TEM Cu grid. STEM data were obtained using a JEM-ARM 200CF (JEOL, Japan) equipped with a fifth-order spherical aberration (C_s) corrector (ASCOR, CEOS GmbH, Germany) at the Materials Imaging and Analysis Center of POSTECH in South Korea. The acceleration voltage was 200 kV, and a HAADF detector was used to acquire the STEM images. EDS elemental mapping was acquired by dual-EDS (JEOL, Japan) silicon drift detectors.

HER Measurements. HER measurements were performed using a three-electrode system in an acidic electrolyte (0.5 M H_2SO_4 solution), with Au, Ag/AgCl, and Pt as working, reference, and counter electrodes, respectively. To study the catalytic effect of MoS_2, MoS_2 flakes with a partial coverage of ∼80% were transferred onto thermally deposited Au thin films with 50 nm thickness. Linear sweep voltammetry measurements were performed on a working electrode that had an area of ∼0.2 cm^2; the scan rate was 2 mV/s, maintained using a potentiostat.

Device Fabrication and Characterization. To fabricate back-gated field-effect transistors, Cr/Au (5/40 nm) electrodes were patterned on degenerately p-doped Si/100 nm SiO_2 substrates by photolithography. Then, as-grown continuous MoS_2 films were transferred onto the prepatterned electrodes, and MoS_2 channels were defined by photolithography and O_2 plasma etching. The photoresists were removed by immersing the samples in acetone for a few hours. Before electrical measurements, the samples were annealed at 200 °C under a vacuum (∼10^{-3} Torr) for an hour. The channel length and width of characterized devices were 20 and 10 μm, respectively. All of the measurements were conducted under vacuum conditions (∼10^{-3} Torr).

ASSOCIATED CONTENT

Supporting Information

The Supporting Information is available free of charge at https://pubs.acs.org/doi/10.1021/acsanm.2c00369.

Chemical compositions and glass transition temperatures of glass substrates; characterization of monolayer MoS_2 films; STEM and EDS data for MoS_2; PL and Raman spectra of sulfurized intermediates; SEM and EDS data for growth intermediates; AFM data for the morphology of eutectic alloys; optical image of a continuous as-grown MoS_2 film; diffusion-limited aggregation model for nucleation; and optical images of MoS_2 by growths at low- and high-condensation regimes (PDF)

AUTHOR INFORMATION

Corresponding Authors

Si-Young Choi − *Department of Materials Science & Engineering, Pohang University of Science and Technology, Pohang 37673, Republic of Korea;* orcid.org/0000-0003-1648-142X; Email: youngchoi@postech.ac.kr

Cheol-Joo Kim − *Department of Chemical Engineering, Pohang University of Science and Technology, Pohang 37673, Republic of Korea;* orcid.org/0000-0002-4312-3866; Email: kimcj@postech.ac.kr

Authors

Min-Yeong Choi − *Department of Chemical Engineering, Pohang University of Science and Technology, Pohang 37673, Republic of Korea;* orcid.org/0000-0001-6966-3513

Chang-Won Choi − *Department of Materials Science & Engineering, Pohang University of Science and Technology, Pohang 37673, Republic of Korea;* orcid.org/0000-0003-3620-7460

Seong-Jun Yang − *Department of Chemical Engineering, Pohang University of Science and Technology, Pohang 37673, Republic of Korea;* orcid.org/0000-0002-7221-0918

Hojeong Lee − *Department of Materials Science & Engineering, Pohang University of Science and Technology, Pohang 37673, Republic of Korea*

Shinyoung Choi − *Department of Chemical Engineering, Pohang University of Science and Technology, Pohang 37673, Republic of Korea;* orcid.org/0000-0001-5465-7719

Jun-Ho Park − *Department of Chemical Engineering, Pohang University of Science and Technology, Pohang 37673, Republic of Korea;* orcid.org/0000-0003-2887-1994

Jong Heo − *Department of Materials Science & Engineering, Pohang University of Science and Technology, Pohang 37673, Republic of Korea*

Complete contact information is available at: https://pubs.acs.org/10.1021/acsanm.2c00369

Author Contributions

[§]M.-Y.C. and C.-W.C. contributed equally to this work. M.-Y.C. and C.-J.K. designed the experiments. C.-W.C. and S.-Y.C. performed the TEM and STEM-EDS imaging and data analysis. S.-J.Y. performed DF-TEM imaging. H.L. and J.H. prepared the glass substrates for the growths. M.-Y.C. grew MoS_2 samples. J.-H.P., S.-J.Y., and S.C. assisted device

https://doi.org/10.1021/acsanm.2c00369
ACS Appl. Nano Mater. 2022, 5, 4336−4342

fabrications and electrical and optical measurements. C.-J.K. and M.-Y.C. wrote the manuscript with input from all authors.

Notes

The authors declare no competing financial interest.

■ ACKNOWLEDGMENTS

This work was supported by a research program funded by Samsung Electronics Co., Ltd., the Basic Science Research Program (2020R1C1C1014590), the Basic Research Laboratory Program (2020R1A4A1019455), and the Creative Materials Discovery Program (2018M3D1A1058793 and 2020M3D1A1110548) of the National Research Foundation of Korea (NRF) funded by the Korea government (Ministry of Science and ICT). C.-W.C. and S.-Y.C. acknowledge the Korea Basic Science Institute (National Research Facilities and Equipment Center) grant funded by the Ministry of Education (2020R1A6C101A202).

■ REFERENCES

(1) Kang, K.; Xie, S.; Huang, L.; Han, Y.; Huang, P. Y.; Mak, K. F.; Kim, C. J.; Muller, D.; Park, J. High-Mobility Three-Atom-Thick Semiconducting Films with Wafer-Scale Homogeneity. *Nature* **2015**, *520*, 656−660.

(2) Wang, Y.; Kim, J. C.; Wu, R. J.; Martinez, J.; Song, X.; Yang, J.; Zhao, F.; Mkhoyan, A.; Jeong, H. Y.; Chhowalla, M. Van Der Waals Contacts between Three-Dimensional Metals and Two-Dimensional Semiconductors. *Nature* **2019**, *568*, 70−74.

(3) Nasr, J. R.; Simonson, N.; Oberoi, A.; Horn, M. W.; Robinson, J. A.; Das, S. Low-Power and Ultra-Thin MoS_2 Photodetectors on Glass. *ACS Nano* **2020**, *14*, 15440−15449.

(4) Amani, M.; Lien, D.-H.; Kiriya, D.; Xiao, J.; Azcatl, A.; Noh, J.; Madhvapathy, S. R.; Addou, R.; KC, S.; Dubey, M.; Cho, K.; Wallace, R. M.; Lee, S.-C.; He, J.-H.; Ager, J. W.; Zhang, X.; Yablonovitch, E.; Javey, A. Near-Unity Photoluminescence Quantum Yield in MoS_2. *Science* **2015**, *350*, 1065−1068.

(5) Liu, X.; Guo, Q.; Qiu, J. Emerging Low-Dimensional Materials for Nonlinear Optics and Ultrafast Photonics. *Adv. Mater.* **2017**, *29*, No. 1605886.

(6) Zuo, Y.; Yu, W.; Liu, C.; Cheng, X.; Qiao, R.; Liang, J.; Zhou, X.; Wang, J.; Wu, M.; Zhao, Y.; Gao, P.; Wu, S.; Sun, Z.; Liu, K.; Bai, X.; Liu, Z. Optical Fibres with Embedded Two-Dimensional Materials for Ultrahigh Nonlinearity. *Nat. Nanotechnol.* **2020**, *15*, 987−991.

(7) Zhu, J.; Wang, Z. C.; Dai, H.; Wang, Q.; Yang, R.; Yu, H.; Liao, M.; Zhang, J.; Chen, W.; Wei, Z.; Li, N.; Du, L.; Shi, D.; Wang, W.; Zhang, L.; Jiang, Y.; Zhang, G. Boundary Activated Hydrogen Evolution Reaction on Monolayer MoS_2. *Nat. Commun.* **2019**, *10*, No. 1348.

(8) Yang, P.; Zou, X.; Zhang, Z.; Hong, M.; Shi, J.; Chen, S.; Shu, J.; Zhao, L.; Jiang, S.; Zhou, X.; Huan, Y.; Xie, C.; Gao, P.; Chen, Q.; Zhang, Q.; Liu, Z.; Zhang, Y. Batch Production of 6-inch Uniform Monolayer Molybdenum Disulfide Catalyzed by Sodium in Glass. *Nat. Commun.* **2018**, *9*, No. 979.

(9) Xie, C.; Yang, P.; Huan, Y.; Cui, F.; Zhang, Y. Roles of Salts in the Chemical Vapor Deposition Synthesis of Two-Dimensional Transition Metal Chalcogenides. *Dalton Trans.* **2020**, *49*, 10319−10327.

(10) Kim, H.; Ovchinnikov, D.; Deiana, D.; Unuchek, D.; Kis, A. Suppressing Nucleation in Metal-Organic Chemical Vapor Deposition of MoS_2 Monolayers by Alkali Metal Halides. *Nano Lett.* **2017**, *17*, 5056−5063.

(11) Wang, P.; Lei, J.; Qu, J.; Cao, S.; Jiang, H.; He, M.; Shi, H.; Sun, X.; Gao, B.; Liu, W. Mechanism of Alkali Metal Compound-Promoted Growth of Monolayer MoS_2: Eutectic Intermediates. *Chem. Mater.* **2019**, *31*, 873−880.

(12) Huang, L.; Thi, Q. H.; Zheng, F.; Chen, X.; Chu, Y. W.; Lee, C. S.; Zhao, J.; Ly, T. H. Catalyzed Kinetic Growth in Two-Dimensional MoS_2. *J. Am. Chem. Soc.* **2020**, *142*, 13130−13135.

(13) Li, S.; Lin, Y. C.; Zhao, W.; Wu, J.; Wang, Z.; Hu, Z.; Shen, Y.; Tang, D. M.; Wang, J.; Zhang, Q.; Zhu, H.; Chu, L.; Zhao, W.; Liu, C.; Sun, Z.; Taniguchi, T.; Osada, M.; Chen, W.; Xu, Q. H.; Wee, A. T. S.; Suenaga, K.; Ding, F.; Eda, G. Vapour-Liquid-Solid Growth of Monolayer MoS_2 Nanoribbons. *Nat. Mater.* **2018**, *17*, 535−542.

(14) Gnanasekaran, T.; Mahendran, K. H.; Kutty, K.V.G.; Mathews, C. K. Phase Diagram Studies on The Na-Mo-O System. *J. Nucl. Mater.* **1989**, *165*, 210−216.

(15) Chang, M. C.; Ho, P. H.; Tseng, M. F.; Lin, F. Y.; Hou, C. H.; Lin, I. K.; Wang, H.; Huang, P. P.; Chiang, C. H.; Yang, Y. C.; Wang, I. T.; Du, H. Y.; Wen, C. Y.; Shyue, J. J.; Chen, C. W.; Chen, K. H.; Chiu, P. W.; Chen, L. C. Fast Growth of Large-Grain and Continuous MoS_2 Films through a Self-Capping Vapor-Liquid-Solid Method. *Nat. Commun.* **2020**, *11*, No. 3682.

(16) Najmaei, S.; Liu, Z.; Zhou, W.; Zou, X.; Shi, G.; Lei, S.; Yakobson, B. I.; Idrobo, J. C.; Ajayan, P. M.; Lou, J. Vapour Phase Growth and Grain Boundary Structure of Molybdenum Disulphide Atomic Layers. *Nat. Mater.* **2013**, *12*, 754−759.

(17) van der Zande, A. M.; Huang, P. Y.; Chenet, D. A.; Berkelbach, T. C.; You, Y.; Lee, G.-H.; Heinz, T. F.; Reichman, D. R.; Muller, D. A.; Hone, J. C. Grains and Grain Boundaries in Highly Crystalline Monolayer Molybdenum Disulphide. *Nat. Mater.* **2013**, *12*, 554−561.

(18) Wu, S.; Huang, C.; Aivazian, G.; Ross, J. S.; Cobden, D. H.; Xu, X. Vapor−Solid Growth of High Optical Quality MoS_2 Monolayers with Near-Unity Valley Polarization. *ACS Nano* **2013**, *7*, 2768−2772.

(19) Zhan, Y.; Liu, Z.; Najmaei, S.; Ajayan, P. M.; Lou, J. Large-Area Vapor-Phase Growth and Characterization of MoS_2 Atomic Layers on a SiO_2 Substrate. *Small* **2012**, *8*, 966−971.

(20) Lei, J.; Xie, Y.; Yakobson, B. I. Gas-Phase "Prehistory" and Molecular Precursors in Monolayer Metal Dichalcogenides Synthesis: The Case of MoS_2. *ACS Nano* **2021**, *15*, 10525−10531.

(21) Voorhees, P. W. The Theory of Ostwald Ripening. *J. Stat. Phys.* **1985**, *38*, 231−252.

(22) Madras, G.; McCoy, B. J. Temperature Effects during Ostwald Ripening. *J. Chem. Phys.* **2003**, *119*, 1683−1693.

(23) Pratontep, S.; Nüesch, F.; Zuppiroli, L.; Brinkmann, M. Comparison between Nucleation of Pentacene Monolayer Islands on Polymeric and Inorganic Substrates. *Phys. Rev.* **2005**, *72*, No. 085211.

(24) Choi, S.; Nguyen, N. N.; Lee, Y.; Yang, S. J.; Kim, K.; Cho, K.; Kim, C. J. Nanoscale Molecular Building Blocks for Layer-by-Layer Assembly. *Adv. Mater. Interfaces* **2020**, *7*, No. 2000522.

(25) Shang, S. L.; Lindwall, G.; Wang, Y.; Redwing, J. M.; Anderson, T.; Liu, Z. K. Lateral Versus Vertical Growth of Two-Dimensional Layered Transition-Metal Dichalcogenides: Thermodynamic Insight into MoS_2. *Nano Lett.* **2016**, *16*, 5742−5750.

(26) Zhang, P.; Kim, Y. H. Understanding Size-Dependent Morphology Transition of Triangular MoS_2 Nanoclusters: The Role of Metal Substrate and Sulfur Chemical Potential. *J. Phys. Chem. C* **2017**, *121*, 1809−1816.

(27) Singh, A.; Moun, M.; Sharm, M.; Barman, A.; Kumar Kapoor, A.; Singh, R. NaCl-assisted Substrate Dependent 2D Planar Nucleated Growth of MoS_2. *Appl. Surf. Sci.* **2021**, *538*, No. 148201.

https://doi.org/10.1021/acsanm.2c00369
ACS Appl. Nano Mater. 2022, 5, 4336−4342